J Fluoresc (2008) 18:297–303
DOI 10.1007/s10895-007-0269-y

ORIGINAL PAPER

Effect of Polymer Strengtheners on the Local Environment of Biocompatible Glass as Probed by Fluorescence

Graham Hungerford · Mariana Amaro · Pedro Martins · M. Isabel Ferreira · Mahesh Uttamlal · A. Sheila Holmes-Smith

Received: 22 June 2007 / Accepted: 8 October 2007 / Published online: 23 November 2007

Abstract Mixed silica–calcite matrices were prepared by developing a "low" temperature (sol–gel) method in presence of several biocompatible polymers, thus providing samples with adequate porosity for the flow of biological fluids and also mechanically robust. In order to analyse and characterise the sample's microenvironments, the highly solvatochromic probe Nile red was used, which enabled the role of polymer addition upon local environmental effects in the host media to be elucidated. The polymers used were polyethylene glycol, polymethylmethacrylate and polyethylene. Each matrix was also characterized with respect to microstructure, morphology and pore size via the use of X-ray diffractometry and scanning electron microscopy.

The results show that is was possible to obtain, in a controlled way, mixed silica–calcite matrices with a wide range of porosities (important if the material is to be used for scaffold or drug release applications, for example). The spectroscopic behaviour of Nile red when incorporated has confirmed the existence of distinct and specific local polarities within each type of matrix that may determine to a large extent the mechanism of interaction between these matrices and biological molecules.

Keywords Silica–calcite matrices · Biocompatible polymers · Photoluminescence methods

Introduction

In recent years, the application of photoluminescence methods to biomedical sciences has proved very successful, as shown by the innumerable scientific publications of the last decade. In fact, the high sensitivity of molecular fluorescence to its environment makes it possible to probe complex environments and/or materials from a wide range of aspects; local polarity effects, specific physical and chemical interactions, and also morphological and topological constraints [1–4]. In the field of biocompatible materials, with the development of new materials, it is now possible to produce bioactive glasses for the purpose of bone tissue scaffolds by many ways [5]. Most methods involve high temperatures when creating the matrix via a sintering phase [6]. However, it is possible to produce this type of material by the sol–gel technique, through a direct method at significantly lower temperatures [7]. This is important as it avoids the problem of temperature degradation when incorporating probes or biological materials, such as proteins, during matrix production.

In the present work, mixed silica–calcite matrices were prepared by developing a "low" temperature (sol–gel) method in presence of several biocompatible polymers, thus providing samples with adequate porosity for the flow of biological fluids and also mechanically robust. It is therefore essential to investigate how these hybrid materials

Electronic supplementary material The online version of this article (doi:10.1007/s10895-007-0269-y) contains supplementary material, which is available to authorized users.

G. Hungerford (✉) · M. Amaro · P. Martins · M. I. Ferreira
Centro de Física, Universidade do Minho,
4710-057 Braga, Portugal
e-mail: graham@fisica.uminho.pt

M. Uttamlal · A. S. Holmes-Smith
School of Engineering, Science and Design,
Glasgow Caledonian University,
Cowcaddens Road,
Glasgow G4 0BA Scotland, UK

will interact with biological molecules and thus knowledge on the local environments (within the matrix) and how these can affect any adsorbed protein is essential.

In order to analyse and characterise the sample's micro-environments, the probe Nile red (NR) was used. Nile red is a fluorescent dye that displays a spectroscopic behaviour largely dependent upon the polarity of the host medium [8], thus providing elucidation on the role of polymer addition upon local environmental effects in the host media. The polymers used were polyethylene glycol (PEG), polymethylmethacrylate (PMMA) and polyethylene (PE). Each matrix was also characterized with respect to microstructure, morphology and pore size.

The results show that is was possible to obtain, in a controlled way, mixed silica–calcite matrices with a wide range of porosities. The control over pore size was achieved due to its importance if the material is to be used for scaffold or drug release applications, for example. The spectroscopic behaviour of NR when incorporated has confirmed the existence of distinct and specific local polarities within each type of matrix that may determine to a large extent the mechanism of interaction between these matrices and biological molecules, namely proteins, in further applications.

Experimental

Sample preparation

Nile red (NR), tetra-ethoxysilane (TEOS), calcium nitrate ($Ca(NO_3)_2{\cdot}4H_2O$), sodium bicarbonate ($NaHCO_3$), sodium hydrogen pyrophosphate ($Na_2H_2P_2O_7$) and calcium carbonate ($CaCO_3$) were purchased from Aldrich Chemical Co. Inc and used without further purification. Polyethylene glycol (PEG; Mwt 400 and 1,000), polymethyl methacrylate (PMMA) and low density polyethylene (PE) were also supplied by Aldrich Chemical Co. Inc. and used as received. All solvents were of spectroscopic grade.

SiO_2 based sol–gel matrices were prepared by an acid-catalyzed sol–gel technique, identical to the one reported by Hall et al. [7], in presence of calcium nitrate. In the early stages of the gelation process, sodium bicarbonate-sodium hydrogen phosphate and calcium carbonate were added, followed by NR addition. Polymer addition was also performed at this stage.

At the end of the gelation process, a few samples were treated with HCl (1 M) in order to attempt removal of the added calcium carbonate and therefore promote sample porosity. Samples treated with HCl are referred to as Si/Ca (AT) whereas samples not treated as Si/Ca. Samples prepared with NR incorporation are referred to as NR-Si/Ca. Throughout, hybrid matrices, prepared by the addition of a polymer, will be referred to as Si/Ca/POL. For example, NR-Si/Ca/PMMA will represent a sample prepared with the addition of NR and the polymer polymethyl methacrylate. All samples were prepared as porous and opaque monoliths (~7×7×15 mm) with copies made to check the reproducibility of the results.

Sample characterisation

X-ray diffractometry (XRD) was performed by means of a Philips PW 1710 diffractometer with the samples first reduced to a powder. Scanning electron microscopy (SEM) was performed on samples coated with gold/palladium on a Polaron SC7640 sputter coater, using a Carl Zeiss EVO50 microscope. Energy dispersive spectroscopy involved the use of an EDAX Genesis 4000 system associated with the electron microscope. Matrix densities were obtained from weighing each sample. Porosities of all samples, were estimated according to the stoichiometry of the chemical processes involved and considering each matrix as composed by a porous mixture of two components (SiO_2 and $CaCO_3$) or three components (SiO_2, $CaCO_3$ and polymer).

Spectroscopic measurements

In view of the samples opaqueness, absorption spectra of NR were obtained from the measurement of diffuse reflectance spectra on a Shimadzu 3101 PC by means of the Kubelka–Munk theory. According to this theory [9, 10], the light flux in a thin layer of a medium containing light absorbing and scattering particles are described by the following equations:

$$dI = -(K + S)I dx + SJ dx \quad (1)$$

$$dJ = (K + S)J dx - SI dx \quad (2)$$

where I and J are the light flux away from and towards the surface, respectively, as shown in scheme below, for a thin layer of thickness dx at the a depth x. K and S are the absorption and scattering coefficients of the sample, respectively.

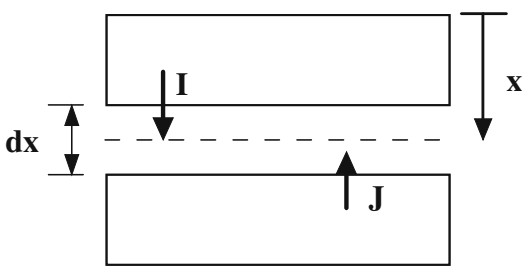

For thick samples, where the light penetrates up to depths much smaller than the sample thickness, Eqs. 1 and 2 can be solved in the Kubelka–Munk approximation, e.g.,

$$\frac{(1-R^2)}{2R} = \frac{K}{S} \tag{3}$$

According to Eq. 3, the measured reflectance R is related to K and S. Therefore it is possible to obtain spectra directly proportional to K from the measurement of R.

Reflectance spectra were recorded in the range 250–2,000 nm, however spectral analysis was performed in the range 400–650 nm, which corresponds to the region where there is significant absorption of NR. The standard used for the reflectance measurements was a sample of freshly compressed barium sulphate ($BaSO_4$) powder.

Fluorescence emission, excitation and synchronous spectra were recorded on a Fluorolog 3, from HORIBA Jobin Yvon. Emission spectra were obtained in the front face configuration. In order to assess the presence of local effects, emission spectra were decomposed as a sum of n Gaussian bands, according to

$$I(E) = \sum_{i=1}^{n} \frac{Ai}{\sqrt{2\pi}\,\gamma i} e^{-(E-E_i)^2/2\gamma_i^2} \tag{4}$$

using Microcal Origin software. Best fits were obtained by minimizing the residues of each fitting procedure, defined as:

$$\varphi = \left(\frac{\sum \left(I_{\text{exp}} - I_{\text{cal}}\right)^2}{\sum \left(I_{\text{exp}}\right)^2} \right)^{1/2} \tag{5}$$

Fluorescence decay times were measured by means of a single-photon counting apparatus equipped with LED excitation source with a peak emission at 495 nm, (HORIBA, Jobin Yvon). Cut-off filters were used to select the emission signal then detected using a Hamamatsu R-2949 side-window photomultiplier. Data were analysed as the sum of exponential decays, according to equation,

$$I(t) = \sum_{i=1}^{n} \alpha_i \exp(-t/\tau_i) \tag{6}$$

using IBH DAS6 software. The goodness of each fit is expressed in terms of χ^2. Errors are given as three standard deviations. All measurements were performed at room temperature.

Results and discussion

Matrix characterisation studies

X-ray diffractograms are shown in Fig. 1 for the following samples; A, B, C, D, E and H. Diffractograms of samples Si/Ca (without polymer addition) show that, in every case, the final matrix is composed by the superimposition of two networks; amorphous silica, identical to opal and calcium carbonate in the form of well defined calcite crystals. No other form of calcium is found. The XRD spectra also show that the acid treatment did not remove a significant part of the calcium carbonate (added or produced). This is confirmed by measurements on matrix density and corresponding porosity, as shown in Table 1 for samples A and B. It is interesting to note that addition of PEG, PMMA or PE does not alter the structural characteristics of the silica and the calcite networks. The SEM data show that the samples have pores that range in size from 20 to 200 μm and elemental analysis by SEM-EDX confirmed the presence of the two co-existing networks, as can be seen in Fig. 2. This shows the spatial separation of Si and Ca containing networks, with the smoother Si network contrasting with the rougher Ca one. The study of the effect of polymer addition on the bioactivity of these samples is presently underway and initial studies, performed by immersing samples (A,B,C) in simulated body fluid, have indicated the growth of calcium phosphate aggregates [11].

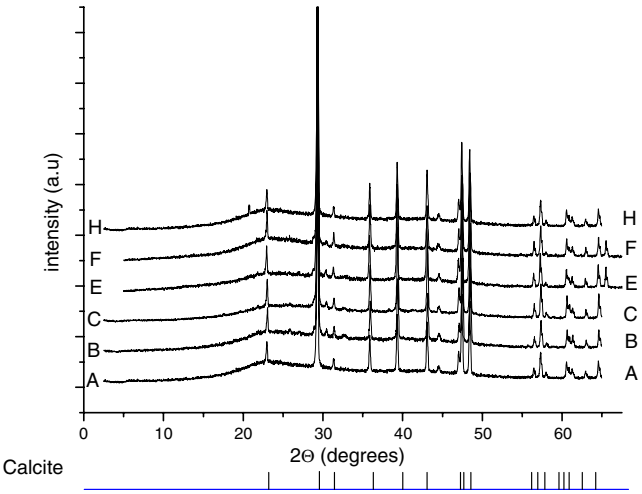

Fig. 1 X-ray diffractograms of different polymer containing samples, along with the expected line positions for synthetic calcite for reference. Compositions; *A* [NR-Si/Ca (AT)], *B* (NR-Si/Ca), *C* [NR-Si/Ca(hp)], *E* (NR-Si/Ca/PMMA), *F* (NR-Si/Ca/PEG 400), *H* (NR-Si/Ca/PE). The spectra are shown offset vertically for clarity

Table 1 summarises all data on matrix characterisation. It shows that samples with identical structure but with a wide range of porosities could be prepared. Highly porous samples, such as sample C, were found to be brittle. All samples used for spectroscopic studies were of lower porosities since they showed better mechanical stability and were optically more homogeneous.

Reflectance and emission studies

Absorption spectra of NR incorporated into all samples were obtained from diffuse reflectance measurements in the range 400–650 nm, as described previously. It was possible

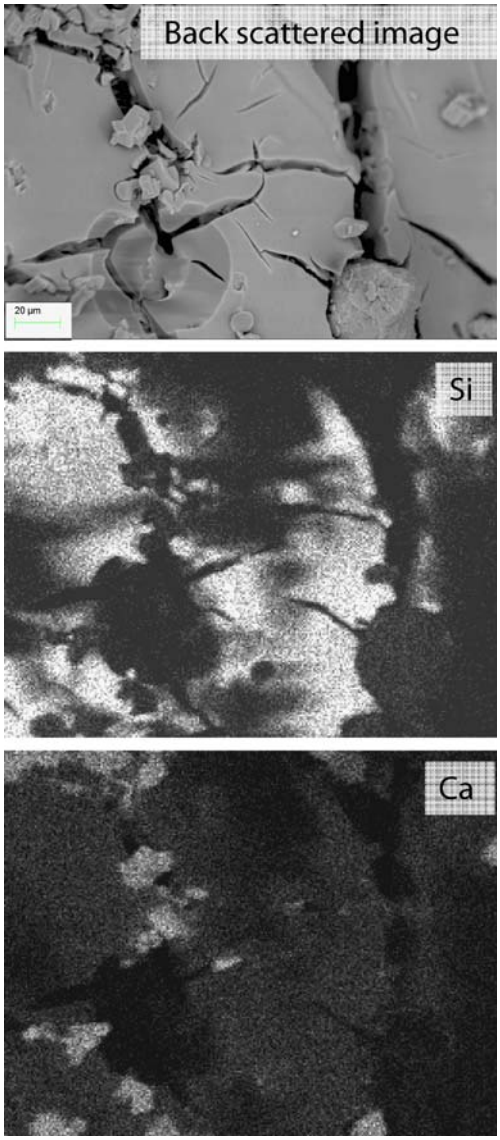

Fig. 2 SEM and EDS map showing difference between Si and Ca areas for sample **G**

to apply the Kubelka–Munk theory to all samples. In fact, not only all samples were opaque, but also the Stokes shift between absorption and emission spectra was always in the order of at least 50 nm thus precluding the interference of the emission on the reflectance spectra. Fig. 3 shows representative absorption spectra. All spectra show no vibronic structure which indicates that NR probes polar environments in all samples, according to previous studies [12]. The wavelength corresponding to the maximum of the broad absorption band in each spectrum is shown in Table 1 for all samples. According to these data, the absorption maxima occurs in the range 590–610 nm for all samples except E and H to which PMMA and PE were added, respectively. In the case of these samples the absorption maxima occur at 534 nm for E and 575 nm for H, that is, considerably blue-shifted as compared with all the remaining samples.

The fluorescence spectra, as shown in Fig. 4 show a trend similar to the absorption spectra since the emissions do not show vibronic structure. Moreover, spectra pertaining to samples E and H present emission spectra that are blue-shifted as compared the other samples. It is interesting to note that these two samples also present a higher carbon contain, relating to polymer presence, as observed via SEM analysis (see Electronic Supplementary Material). Absorption and emission spectra of NR when incorporated into a Si/Ca matrix (sample D) display features characteristic of polar environments in that both absorption and fluorescence spectra do not show apparent vibronic structure but a broad band with absorption and emission maxima occurring at 604 and 665 nm, respectively, as shown in Table 1. Such behaviour indicates that NR probes significantly polar and "homogeneous" micro-environments. This interpretation is further corroborated by the corresponding emission spectra recorded for the same sample but in the synchronous scan data acquisition mode [13, 14], shown in Fig. 5. From previous studies by some of the authors [12], it has been shown that the solvatochromic properties of NR are dominated by electronic relaxation and to a minor extent by dipole reorientation of the environment.

It has been well established by several authors [15, 16] that Eq. 7 correlates, to a good approximation, the spectral shifts in the emission spectra, (by reference to the vapor phase spectrum, E_F^O) with local effects produced by electronic and dipolar relaxation.

$$\Delta E_F = E_F - E_F^0 = C_1 \frac{n^2-1}{2n^2+1} + C_2\left(\frac{\varepsilon-1}{\varepsilon+2} - \frac{n^2-1}{n^2+2}\right) \tag{7}$$

Where $\frac{n^2-1}{2n^2+1} = f(n^2)$ refers to the redistribution of electrons, whereas the other term, $f(\varepsilon, n^2)$, refers to the reorientation of dipoles. According to the studies [12] previously referred to, it was found for NR:

$$\begin{aligned} E_F^0 &= 2.649\text{eV}(487\text{nm}) \\ C_1 &= -1.128\text{eV} \\ C_2 &= -0.556\text{eV} \end{aligned} \tag{8}$$

It is therefore possible to estimate the spectral shift in NR emission peak that results from a general solvatrochromic effect caused by any known environment. In the case of NR dispersed in bulk SiO_2 (n=1.54 and ε=3.8 [17]) a red shift of 0.364 eV is predicted from Eq. 7 whereas a red shift of 0.456 eV is predicted for NR in bulk $CaCO_3$ (n=1.486, ε= 6.14, from [3]). In both cases the calculated shifts are significantly lower than the experimentally observed emission maximum for NR-Si/Ca. Therefore, the high polar environment probed by NR in this matrix most probably originates from hydroxyl groups present in the silica-gel

Table 1 Data obtained from matrix characterisation, reflectance and emission studies

Sample	Composition	Porosity	λ_{abs}^{max} (nm)	λ_{em}^{max} (nm)	τ_F (ns)	α	χ^2
A	Si/Ca (AT)	0.52					
B	Si/Ca	0.41					
C	Si/Ca (hp)	0.73					
D	NR-Si/Ca	0.44	604	665	0.35±0.19	−0.51	1.19
					3.02±0.06	0.46	
					6.14±0.21	0.03	
E	NR-Si/Ca/PMMA	0.50	534	603	0.21±0.02	−0.35	1.13
					3.01±0.03	−0.16	
					4.95±0.02	0.49	
F	NR-Si/Ca/PEG 400	0.40	604	663	0.22±0.02	−0.51	1.19
					3.52±0.09	0.42	
					5.69±0.12	0.07	
G	NR-Si/Ca/PEG 1000	0.43	602	660	0.46±0.01	−0.47	1.19
					3.95±0.04	0.52	
					10.8±1.0	0.01	
H	NR-Si/Ca/PE	0.53	575	623	0.18±0.02	−0.51	1.21
					2.78±0.31	0.30	
					4.16±0.08	0.18	

Emission spectra were recorded with excitation at 490 nm. Porosities are expressed as fractions per unit volume.

lattice as previously reported by several authors [18, 19]. In the presence of the hydroxyl groups, a common feature in these matrices, the effective dielectric constant probed by NR should achieve significantly higher values as compared with bulk SiO_2.

The emission decay of sample D (NR-Si/Ca) was best fitted to a three exponential decomposition, as shown in Table 1. Theses results are in agreement with the work of Krishna [20], in that the fast component is associated with a negative amplitude whereas the second component, longer lived, is associated with a positive amplitude thus confirming the existence of an initially excited state (the short-lived) that is converted into a second, longer lived excited state. A minor third and longer lived component is found in the present work; it could arise from NR molecules entrapped into pores containing retained solvent, mostly ethanol and water [21]. In fact, although the sample porosity is in the order of 44%, residual solvent retention cannot be ruled out. Moreover it is to be expected solvent micro-viscosities in such porous media much higher than in bulk solution [22] thus explaining the longer lived component.

It is interesting to note that addition of PEG does not significantly alter the photophysical behaviour of NR, as shown in Figs. 4 and 5 and also from the analysis of the fluorescence decays measured for NR-Si/Ca-PEG (samples F and G). In fact, also in the case of NR-Si/Ca-PEG samples, the emission decays were best fitted to a three exponential decomposition (Table 1 of Electronic Supplementary Material), with identical features to the NR-Si/Ca sample. Although PEG is a well known agent for the modification of the dielectric constant of aqueous media [23], in the present case this effect is strongly attenuated. Most probably PEG binds quite strongly to calcium ions [24]. This effect precludes further interaction with NR and the hydroxyl groups of the silica network.

Spectral decomposition of emission from samples D (NR-Si/Ca), F (NR-Si/Ca-PEG 400), and G (NR-Si/Ca-PEG 1000) are shown in Fig. 4, and further data concerning the decomposition is given as supplementary information. The best spectral decompositions were obtained with four components; however the fourth component, that occurs at energies ≤1.6 eV (λ≥769 nm), is considered to be less meaningful, since the instrumental response of the fluorimeter is significantly less accurate in this spectral region.

The spectral decomposition leads to identical spectra: one prominent band at 664, 662 and 659 nm for samples D, F and G, respectively, and two minor bands. The emission spectra obtained in the synchronous mode confirm that NR probes a rather "homogenous" and polar environment in these samples.

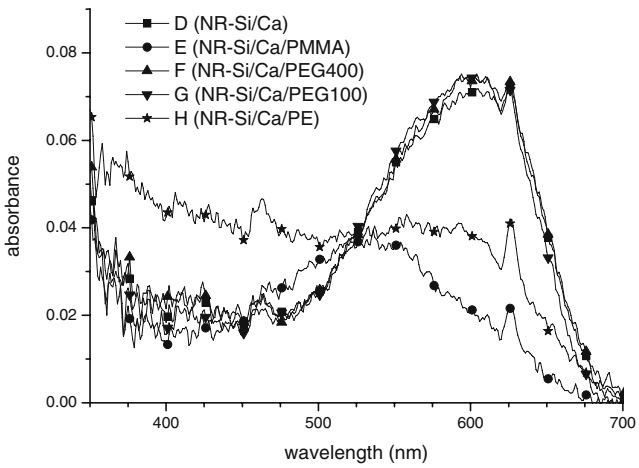

Fig. 3 Absorption of Nile red incorporated within the different samples performed in reflectance mode

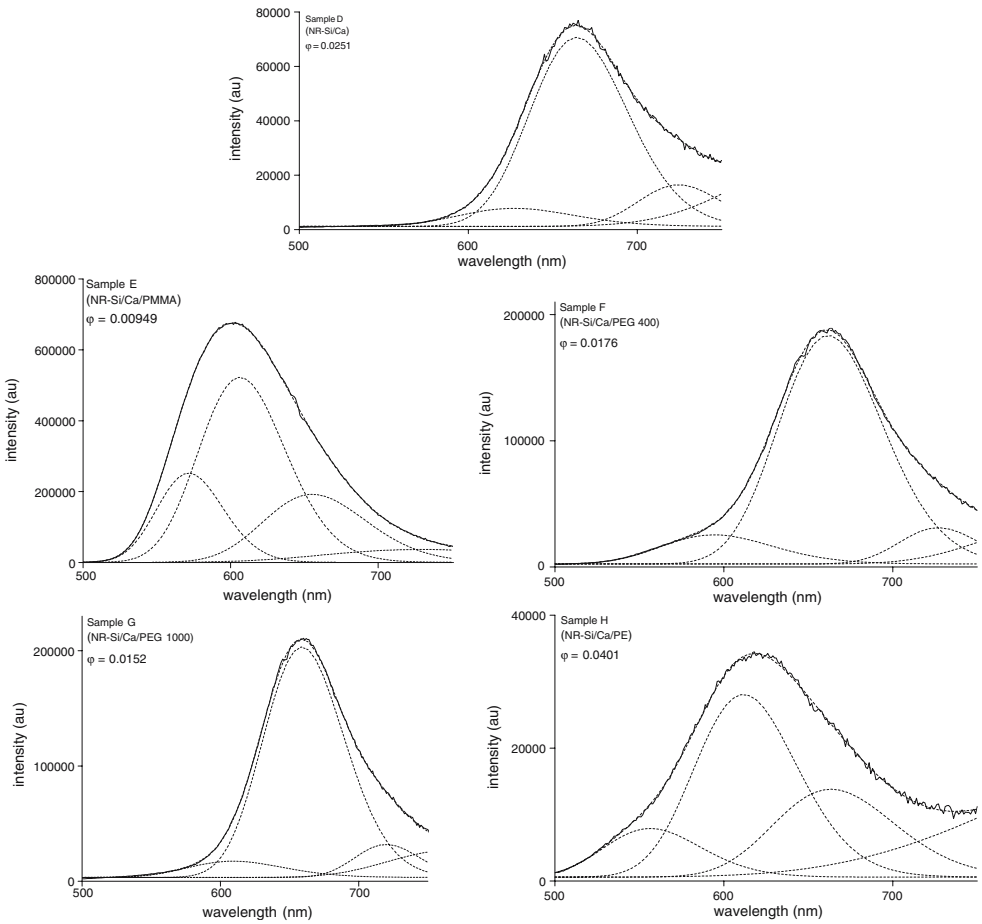

Fig. 4 Fluorescence spectra, excited at 490 nm, showing the decomposition into Gaussian components for Nile red in different polymer containing samples

The behaviour of NR when incorporated into Si/Ca/PMMA (sample E) or Si/Ca/PE (sample H) indicates that, overall, the emission of NR is blue-shifted as compared to the previous samples, as shown in Figs. 4 and 5. This feature indicates that NR probes a significantly less polar environment in these matrices, as compared to the polarity probed by NR in samples D, F and G. In fact, both polymers have dielectric constants in the order of 2.3–2.9 [17].

The emission maximum occurs at 621 nm for sample H (NR-Si/Ca-PE), whereas the prediction for NR in pure PE would be 522 nm, according to Eqs. 7 and 8. The red shift observed experimentally confirms that NR now probes a distinct medium as compared to the samples previously described. In fact, now the synchronous emission (Fig. 5) confirms that NR probes local environments with distinct polarities, in that it reveals two main bands, at 604 and 648 nm. The lower wavelength band originates from NR embedded in a less polar local environment most probably the polymeric PE chain, whereas the band centred at 648 nm is characteristic of NR probing a significantly polar environments, such as the medium probed by NR in sample D (NR-Si/Ca). The relative intensity of these peaks suggests that comparable fractions of NR can be found in each of the local environments detected. The spectral decomposition of the conventional fluorescence spectrum (Fig. 4) shows that the more intense component occurs at 612 nm e.g. blue shifted as compared to the main component of the spectral decomposition of sample D (NR-Si/Ca), centred at 664 nm. The decay analysis confirms the kinetics proposed by Krishna [20].

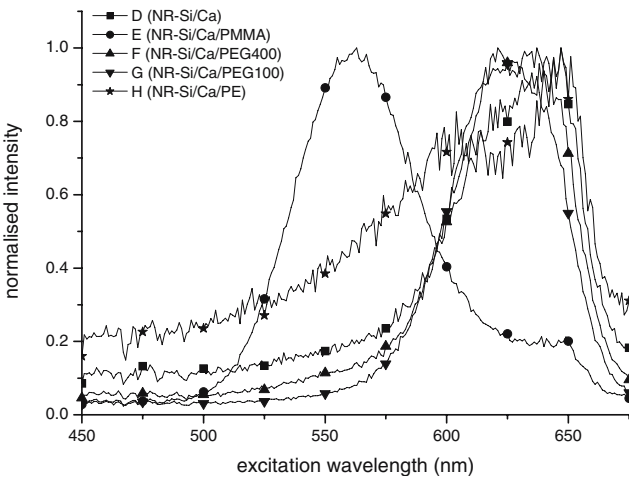

Fig. 5 Synchronous scan of Nile red in the different polymer containing hosts with a 20 nm offset between excitation and emission monochromators

For sample E (NR-Si/Ca-PMMA) the emission maximum of NR occurs at 603 nm, whereas the prediction would be 531 nm, according to Eq. 7 for pure PMMA. Spectral decomposition of this emission, shown in Fig. 4, reveals a major band centred at 606 nm and two somewhat intense bands at 572 and 655 nm. However, the synchronous scan emission spectrum of sample E (NR-Si/Ca-PMMA) shows that, in PMMA, NR is preferentially found in the low polar (PMMA) media with a maximum at 562 nm, but a fraction of NR can also be found in more polar environments, as expressed by the emission band centred at 644 nm. The hydrophobic properties of NR [25, 26] explain its tendency to occupy sites in the vicinity of the PMMA polymeric chains, thus avoiding to a significant extent the hydrophilic (and more polar) sites of the matrix.

Such behaviour is in agreement with the emission decay analysis. In fact the emission lifetime now reveals two components (0.21 and 3.01 ns) with negative amplitude and a third component (4.95 ns) with positive amplitude, thus suggesting the existence of at least two distinct initial excited states that decay both to the longer lived component.

Conclusion

In the present work the fluorescence of the solvatochromic dye Nile red (NR) was studied in order to characterize the local polarities of mixed silica–calcite porous glasses, prepared by a low temperature sol–gel method. Several biocompatible polymers (PE, PEG and PMMA) were also incorporated into some samples to improve their mechanical robustness. It has been shown that the spectroscopic behaviour of NR has confirmed the existence of distinct and specific local environments within each type of matrix.

X-ray diffractometry and electron microscopy have shown that the final sol–gel matrix in every case is composed by the superimposition of two networks: amorphous silica, identical to opal and calcium carbonate in the form of well defined calcite crystals. The control over porosity and pore size was explored due to its importance if the material is to be used for scaffold or drug release applications.

Acknowledgement The authors gratefully acknowledge the contribution of Mr. Azevedo of the Earth Sciences Department, Universidade do Minho, in the measurement of the X-ray diffractograms.

References

1. Rolinski OJ, Birch DJS (2002) Structural sensing using fluorescence nanotomography. J Chem Phys 116:10411–10418
2. Miller JN (2005) Fluorescence energy transfer methods in bioanalysis. Analyst 130:265–270
3. Suhling K, Siegel J, Lanigan PMP, Lévêque-Fort S, Webb SED, Phillips D, Davis DM, French PMW (2004) Time-resolved fluorescence anisotropy imaging (TR-FAIM) applied to live cells. Optics Lett 29:584–586
4. Antia M, Islas LD, Boness DA, Baneyx G, Vogel V (2006) Single molecule fluorescence studies of surface-adsorbed fibronectin. Biomaterials 27:679–690
5. Podbielska H, Ulatowska-Jarza A (2005) Sol–gel technology for biomedical engineering. Bull Pol Acad Sci Tech Sci 53:261–271
6. Vallet-Regi M (2001) Ceramics for medical applications. J Chem Soc Dalton Trans 2:97–108
7. Hall SR, Walsh D, Green D, Oreffo R, Mann S (2003) A novel route to highly porous bioactive silica gels. J Mater Chem 13:186–190
8. Hungerford G, Rei A, Ferreira MIC (2005) Studies on the interaction of Nile red with horseradish peroxidase in solution. FEBS J 272:6161–6169
9. Kubelka P (1948) New Contributions to the Optics of Intensely Light-Scattering Materials. Part I. JOSA 38:448–451
10. Kubelka P (1954) New Contributions to the Optics of Intensely Light-Scattering Materials Part II: Nonhomogeneous Layers. J Opt Soc Am 44:330–335
11. Holmes-Smith AS, Hungerford G, Uttamlal M, Amaro M, Martins P, Love G, McBrearty L, Ferreira MIC (2007) Scanning Electron Microscopy analysis of sol-gel derived biocompatible glass. Inst Phys Conf Ser (in press)
12. Viseu TMR, Hungerford G, Coelho AF, Ferreira MIC (2003) Dye–host interactions for local effects recognition in homogeneous and nanostructured media. J Phys Chem B 107:13300–13312
13. Rubio S, Gomezhens A, Valcarcel M (1986) Analytical applications of synchronous fluorescence spectroscopy. Talanta 33:633–640
14. Vo-Dinh T (1978) Multicomponent analysis by synchronous luminescence spectrometry. Anal Chem 50:396–401
15. Renge I (2000) Mechanisms of solvent shifts, pressure shifts, and inhomogeneous broadening of the optical spectra of dyes in liquids and low-temperature glasses. J Phys Chem A 104:7452–7463
16. Mataga N, Kubota T (1970) *Molecular interactions and molecular spectra,*. Marcel Dekker, New York
17. Lide DR (2002–2003) *Handbook of chemistry and physics 83th edition,*. CRC, Boca Raton
18. Badjić JD, Kostic NM (2000) Unexpected interactions between sol–gel silica glass and guest molecules. Extraction of aromatic hydrocarbons into polar silica from hydrophobic solvents. J Phys Chem B 104:11081–11087
19. Hench LL, West JK (1990) The sol–gel process. Chem Rev 90: 33–72
20. Krishna MMG (1999) Excited-state kinetics of the hydrophobic probe Nile red in membranes and micelles. J Phys Chem A 103:3589–3595
21. Hungerford G, Suhling K, Ferreira JA (1999) Comparison of the fluorescence behaviour of rhodamine 6G in bulk and thin film tetraethylorthosilicate derived sol–gel matrices. J Photochem Photobiol A 129:71–80
22. Squires TM, Quake SR (2005) Microfluidics: Fluid physics at the nanoliter scale. Rev Modern Physics 77:977–1026
23. Herrmann A, Pratsch L, Arnold K, Lassmann G (1983) Effect of poly (ethylene glycol) on the polarity of aqueous-solutions and on the structure of vesicle membranes. Biochim Biophys Acta 733:87–94
24. Maltesh C, Somasundaran P (1992) Effect of binding of cations to polyethene-glycol on its interactions with sodium dodecyl-sulfate. Langmuir 8:1926–1930
25. Greenspan P, Fowler SD (1985) Spectroscopic studies of the lipid probe, Nile red. J Lipid Res 26:781–789
26. Sackett DL, Wolf J (1987) Nile red as a polarity-sensitive fluorescence probe of hydrophobic protein surfaces. Anal Biochem 167:228–234